ACS APPLIED ENERGY MATERIALS

Article

Cite This: ACS Appl. Energy Mater. 2019, 2, 822−832

www.acsaem.org

NaV_2O_5 from Sodium Ion-Exchanged Vanadium Oxide Nanotubes and Its Efficient Reversible Lithiation as a Li-Ion Anode Material

David McNulty,[†] D. Noel Buckley,[‡,§] and Colm O'Dwyer*[,†,∥,⊥]

[†]School of Chemistry, University College Cork, Cork T12 YN60, Ireland

[‡]Department of Physics and [§]Bernal Institute, University of Limerick, Limerick, V94 T9PX, Ireland

[∥]Micro-Nano Systems Centre, Tyndall National Institute, Lee Maltings, Cork T12 R5CP, Ireland

[⊥]Environmental Research Institute, University College Cork, Lee Road, Cork T23 XE10, Ireland

Supporting Information

ABSTRACT: Efficient synthetic protocols for stable oxide materials as Li-ion battery electrodes are important not only for improving long-term battery performance but also for tackling potential material abundance issues and understanding the nature of ion intercalation for beyond lithium technologies. Oxide anodes are denser, typically, than graphite, leading to a doubling or more of the energy density. Using oxides as lower voltage battery anodes that efficiently and reversibly intercalate cations while avoiding dominating conversion-mode side reactions is much less common. We show that ion-exchanging the molecular templates used to form scrolled, layered vanadium oxide nanotubes (VONTs) with sodium ions allows us to form NaV_2O_5 crystals that behave as Li-ion battery anodes with efficienct capacity retention over 1000 cycles. We also track and analyze the thermal recrystallization of intralayer Na^+ ion-exchange in vanadium oxide nanotubes (Na-VONTs) to NaV_2O_5 by thermogravimetric analysis, X-ray and electron diffraction, transmission and scanning electron microscopy, and infrared spectroscopy. The quantification and understanding of the electrochemical performance of ion-exchanged nanotubes before and after thermal treatment was determined by cyclic voltammetry and galvanostatic cycling. NaV_2O_5 in the form of micro- and nanoparticles demonstrates exceptional capacity retention during long cycle life galvanostatic cycling with Li^+, retaining 93% of its capacity from the 100th to the 1000th cycle, when cycled using an applied specific current of 200 mA/g in a conductive additive and binder-free formulation. Intercalation reactions dominate over much of the voltage range. Conversion mode processes are negligible and the material reversibly lithiates with charge compensation by cation (V) redox. This report offers valuable insight into the use of group I (Li, Na, etc.) elements to make vanadate bronzes as long cycle life and stable Li-ion battery anode materials with higher volumetric energy density.

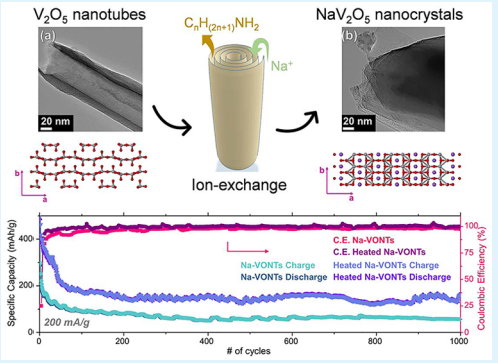

KEYWORDS: *Li-ion battery, anode, sodium vanadate, energy storage, oxide, nanotubes*

INTRODUCTION

Vanadium oxide nanotubes (VONTs) were first reported in 1998 by Spahr et al.[1] and since then has been a great deal of research into how to fully optimize their electrochemical performance as a cathode material for lithium ion (Li-ion) batteries and as an anode using vanadate bronzes and closely related compounds.[2−6] Typically VONTs are prepared by hydrothermal treatment of a vanadium oxide precursor mixed with a primary amine.[7,8] The amine molecules are crucial to the formation of the VONTs as they maintain the vanadium oxide layers which scroll to form the nanotube structure.[9,10] While the amines are vital in the synthesis of the VONTs, they are unfortunately detrimental to their electrochemical performance.[7,10] It has been proposed that the amine molecules occupy the majority of the possible lithium intercalation sites within the VONTs and hence are responsible for the poor cycling performance which has been reported for as-synthesized VONTs.[11] While as-made VONTs exhibit poor electrochemical performance, they are quite useful as a starting structure to provide nanorod or nanowire-type structures with nanoscale features after various post-treatments.[12,13]

The motivating reason to utilize this ion-accessible nanotube structure was to create NaV_2O_5 that is both efficient and stable as a Li-ion battery anode at low voltages, using ion-exchange protocols. Oxides are essentially much denser than graphite and consequently could increase the volumetric energy density if the stable intercalation process is efficient and reversible at low voltages. Some open questions regarding the nature of Li-ion insertion remain and to some degree have been examined for lithium-rich $Li_xV_{1-x}O_2$.[14] Avoiding and mitigating the conversion mode reaction with oxides in Li-containing electrolytes in a battery are also crucial, and vanadium oxides

Received: November 2, 2018
Accepted: January 3, 2019
Published: January 3, 2019

DOI: 10.1021/acsaem.8b01895
ACS Appl. Energy Mater. 2019, 2, 822−832

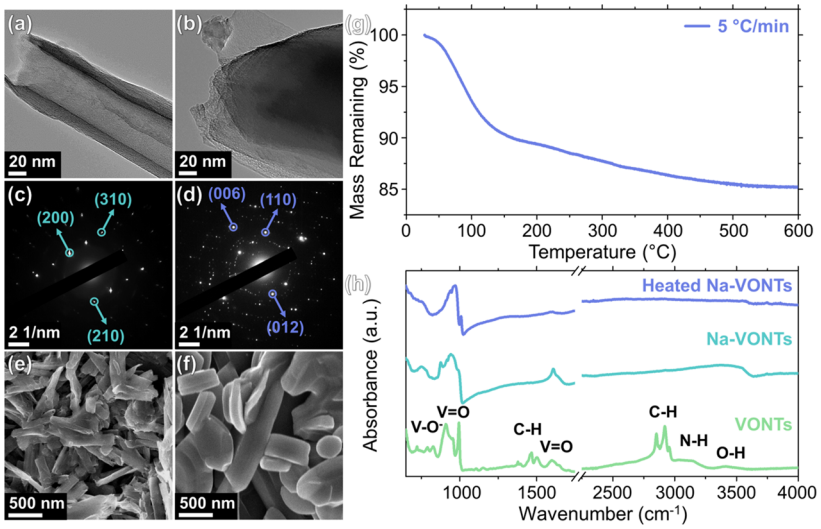

Figure 1. TEM images of (a) Na-VONTs and (b) heated Na-VONTs. Selected area electron diffraction patterns for (c) Na-VONTs and (d) heated Na-VONTs. SEM images of (e) Na-VONTs and (f) Na-VONTs after heating to 600 °C. (g) TGA curve for Na-VONTs heated to 600 °C in N_2, at a heating rate of 5 °C/min. (h) FTIR spectra for as-synthesized VONTs, Na-VONTs, and heated Na-VONTs.

recrystallized into bronzes or polymorphs may behave very well at lower voltages.[15]

In this work we investigate in detail a selective metal cation-exchange reaction method to remove the amine molecules from as-synthesized VONTs, using the nanotube structure as a "backbone" or "starting structure" for other polymorphs, while retaining the nanoscale structure. We confirm the removal of amine molecules and ion-exchange by monitoring the inorganic and organic phase changes and decomposition, using IR spectroscopy, electron microscopy, and X-ray diffraction analyses. By recrystallizing a sodiated VONT (Na-VONT) into the ladder compound NaV_2O_5, a very efficient and stable low-voltage Li-ion battery anode is demonstrated.

Metal cation-exchanged VONTs have been examined before as higher voltage cathode materials for Li-ion batteries, including Ca-VONTs, Fe-VONTs, K-VONTs, and Li-VONTs.[3,5,16,17] Na-VONTs have also been investigated as a cathode material; however, the initial capacities reported were quite low (>60 mAh/g).[2,16] In recent times binary metal oxides containing vanadium such as FeV_2O_4, CoV_2O_6, and $NiVO_3$ have been attracting attention as low voltage anode materials for Li-ion batteries.[15,18,19] Here, we investigate the electrochemical performance of Na^+ ion-exchanged VONTs as an anode material. As the Na-VONTs are heated to 600 °C in N_2, a structural conversion occurs from V_2O_5 with Na^+ intercalated between the VO_x layers to a binary metal oxide in the form of NaV_2O_5. This, to our knowledge, is the first report on both Na-VONTs from which NaV_2O_5 can be used as an intercalation anode material for Li-ion batteries, and as such the work gives valuable insight into the development of vanadates using group I elements larger than Li, as efficient negative electrode materials at lower voltages with higher energy density than graphite. We propose that NaV_2O_5 behaves as an intercalation mode charge storage material, with minimal conversion mode contribution at lower potentials (~0.2 V, vs Li/Li^+). This is evidenced in detailed examination of differential capacity plots (DCPs) of charge curves which reveal a characteristic voltage profile signifying $Li_xNaV_2O_5$ involving cation redox. The heated Na-VONTs demonstrate exceptional capacity retention over long cycle life testing delivering 174 and 162 mAh/g after the 100th and 1000th cycles respectively, when cycled with an applied specific current of 200 mA/g. This corresponds to an impressive capacity retention of >93% over the course of 900 cycles even when cast without conductive additives or F-containing binders within the cell. The capacity values achieved by the heated Na-VONTs are higher than previously reported values for other vanadium oxide-based anode materials including V_2O_3, $Li_{1.1}V_{0.9}O_2$, and Li_3VO_4, thus further exemplifying their beneficial electrochemical behavior.

EXPERIMENTAL SECTION

Synthesis of Vanadium Oxide Nanotubes. Vanadium oxide nanotubes (VONTs) were synthesized by hydrothermal treatment of a mixture of vanadium oxide xerogel and a primary amine, following usual procedures.[9,20,21] Initially, a V_2O_5 xerogel was prepared via a reflux and distillation process as we have previously reported.[12,22,23] V_2O_5 xerogel was mixed with nonylamine in a molar ratio of xerogel to amine of 1:2, with 3 mL of ethanol added per gram of xerogel. The mixture was stirred at 500 rpm for 1 h, and then 5 mL of deionized water per gram of xerogel was added before being vigorously stirred again for a further 2 h. The xerogel/amine mixture was then allowed to age for 2 days. During this time, the mixture turned white and was then hydrothermally treated in a Teflon-lined autoclave at 180 °C for 7 days. The resulting dark black paste was washed with ethanol and dried using a Buchner funnel.

Preparation of Ion-Exchanged VONTs. Ion-exchanged VONTs were prepared using a modified version of a previously reported method.[24] As-synthesized VONTs were mixed with NaCl in a molar ratio of 1:4 to prepare Na^+-doped VONTs (Na-VONTs). The mixture of powders was stirred in a solution of ethanol and deionized water (4:1 v/v) with 0.2 mL of ethanol being added per mg of VONTs. The solution was stirred for 5 h and then then dried on filter paper using a Buchner funnel. Na-VONTs were heated to 600 °C in N_2 at a ramp rate of 5 °C/min and then held at this temperature for 1 h to determine the influence of heat treatment on the structural and electrochemical properties of the Na-VONTs.

Material Characterization. Transmission electron microscopy (TEM) analysis including bright field and electron diffraction was conducted using a JEOL JEM-2100F TEM operating at 200 kV. SEM analysis was performed using a Hitachi S-4800 at an accelerating voltage of 10 kV. Thermogravimetric analysis (TGA) was performed using a PerkinElmer TGA. Samples for TGA were placed in an

DOI: 10.1021/acsaem.8b01895
ACS Appl. Energy Mater. 2019, 2, 822−832

alumina crucible and heated to 600 °C in a nitrogen atmosphere at a heating rate of 5 °C/min. Fourier transform infrared spectroscopy (FTIR) was conducted on a PerkinElmer series 2000 apparatus in the region of 4000−650 cm^{-1}. X-ray diffraction (XRD) analysis was performed using an X'pert MRDpro Panalytical diffractometer with Cu Kα radiation (Cu Kα, λ = 0.15418 nm, operation voltage 40 kV, current 30 mA). X-ray photoelectron spectroscopy (XPS) spectra were acquired on an Oxford Applied Research Escabase XPS system equipped with a CLASS VM 100 mm mean radius hemispherical electron energy analyzer with multichannel detectors in an analysis chamber with a base pressure of 5.0×10^{-10} mbar. Survey scans were recorded between 0 and 1400 eV with a step size of 0.7 eV, dwell time of 0.5 s, and pass energy of 100 eV. Core level scans were acquired with a step size of 0.1 eV, dwell time of 0.5 s, and pass energy of 20 eV averaged over 10 scans. A nonmonochromated Al Kα X-ray source at 200 W power was used for all scans. All spectra were acquired at a takeoff angle of 90° with respect to the analyzer axis and were charge corrected with respect to the C 1s photoelectric line. Data were processed using CasaXPS software where a Shirley background correction was employed and peaks were fitted to Voigt profiles.

Electrochemical Characterization. All electrochemical results presented in this report were performed using a BioLogic VSP potentiostat/galvanostat. The electrochemical properties of Na-VONTs and heated Na-VONTs samples were investigated in a half-cell configuration against a pure Li counter electrode in a two-electrode, stainless steel split cell (a coin cell assembly that can be disassembled for post-mortem analysis). The electrolyte used consisted of a 1 mol dm^{-3} solution of $LiPF_6$ in a 1:1 (v/v) mixture of ethylene carbonate in dimethyl carbonate with 3 wt % vinylene carbonate. The separator used in all split cell tests was a glass fiber separator (El-Cell ECC1-01-0012-A/L, 18 mm diameter, 0.65 mm thickness). The mass loading for all samples was ∼0.5 mg; no additional conductive additives or binders were added. The current collecting substrates were 1 cm^2 pieces of Cu foil. Cyclic voltammetry was performed using a scan rate of 0.1 mV s^{-1} in a potential window of 3.0−0.01 V (vs Li/Li^+). Galvanostatic cycling was performed using a range of specific currents (50−200 mA/g) in a potential window of 3.0−0.01 V (vs Li/Li^+).

RESULTS AND DISCUSSION

Structure of Na^+-Exchanged and Thermally Treated VONTs. TEM images of Na-VONTs and Na-VONTs after heating to 600 °C are shown in Figures 1a and 1b, respectively. There are three main features present in the morphology of as-synthesized VONTs,[7] as can be seen in Figure S1. These are (i) the hollow core running through the nanotube, (ii) the layered walls on either side of the hollow core, and (iii) the tube openings at both ends. After the ion-exchange reaction, Na-VONTs retain the three characteristic nanotube features as seen in Figure 1a. The nanotube structure collapses when Na-VONTs are heated to 600 °C, as shown in Figure 1b. It has previously been suggested that amine molecules act as a structure maintaining template for layers of vanadium oxide during the formation of scrolled VONTs.[7] Partially removing the amine molecules via ion-exchange reactions maintains the overall tubular morphology; however, thermal treatment of Na-VONTs removes any remaining amine molecules, and the nanotube structure collapses. The resulting structures are still layered as can be seen in Figure 1b. Electron diffraction (ED) patterns for Na-VONTs and Na-VONTs heated to 600 °C are shown in Figures 1c and 1d, respectively. The *d*-spacings observed in the ED pattern for the as-prepared VONTs are consistent with previously reported XRD patterns for VONTs.[8,25] The ED pattern for heated Na-VONTs was successfully indexed to pure orthorhombic NaV_2O_5 (JCPDS No. 98-000-0993).

Prior to hydrothermal treatment, during the aging of the mixture of V_2O_5 xerogel and amines, the amines molecules are hydrolyzed to form ammonium ions and hydroxide ions[26] as follows:

$$C_nH_{(2n+1)}NH_2 + H_2O \rightarrow C_nH_{(2n+1)}NH_3^+ + OH^- \quad (1)$$

The hydroxide ions formed reduce the V═O bond present in the layers of V_2O_5 to form V−O^- and V−OH bonds. The attachment of the amine molecules is typically accepted to be an electrostatic bond between the reduced vanadyl (V−O^-) bond and the oxidized amino headgroup (NH_3^+).[20,23,27] During the ion-exchange reaction the positively charged headgroup of the amine molecule is exchanged with a Na^+ ion.[28] However, it is likely to be a partial exchange as amines are structure maintaining templates,[29,30] and as can be seen in Figure 1a,e, the product of the reaction maintains the tubelike structure. If all of the amine molecules were removed, the tubular structure would likely collapse. This can be seen for the case of Na-VONTs heated to 600 °C, as shown in Figure 1b. When Na-VONTs are thermally treated, irregular single crystal nanoparticles are formed, as shown in the SEM image in Figure 1f. TEM and SEM analyses indicate that VONTs and Na-VONTs have a tendency to group together in bundles. As Na-VONTs are annealed to 600 °C, the amines remaining after the ion-exchange reaction are removed, and the nanotube structure collapses. From the dimensions and shapes of the resulting nanostructures from high-resolution microscopy data (Figure 1f), it appears as though bundles of Na-VONTs agglomerate to form these larger nanoparticles.

The thermal stability of Na-VONTs was studied by thermogravimetric analysis (TGA) under a nitrogen atmosphere. The resulting mass loss curve is shown in Figure 1g. Less than 6.5% mass is lost when Na-VONTs are heated to 100 °C, which is associated with the removal of physisorbed and chemisorbed H_2O present within the Na-VONTs. During the ion-exchange reaction as-synthesized VONTs are stirred with NaCl in a mixture of ethanol and distilled water which may have resulted in the presence of physisorbed water on the surface of the Na-VONTs. The total mass loss for Na-VONTs heated to 600 °C was ∼15%, which is considerably lower than the ∼52% mass loss which we previously reported for as-prepared VONTs, heated under the same conditions.[31] This mass loss indicates that a large proportion of amines are removed by the ion-exchange reaction. FTIR measurements were performed to verify the partial exchange of amine molecules with Na^+ ions and to determine the effects of thermal treatment on Na-VONTs structure. The FTIR spectra for as-synthesized VONTs, Na-VONTs, and heated Na-VONTs are shown in Figure 1h. The characteristic vanadyl band (V═O) for crystalline V_2O_5 can be seen at 992 cm^{-1} in the spectra for the as-synthesized VONTs and the Na-VONTs.[32,33] When Na-VONTs are heated to 600 °C, the vanadyl band is shifted to a higher wavenumber (∼1009 cm^{-1}). This modification is from the distortion of the vanadium oxide lattice when accommodating Na^+ ions with a larger ionic radius, which after heat treatment have diffused into the crystal structure of the host material and a change in vanadyl bond length.[34−37] The absorption peak associated with V−O−V asymmetric stretching is observed at 790 cm^{-1} for the as-synthesized VONTs.[17,30] This shifts to ∼760 cm^{-1} for both the Na-VONTs and the thermally treated Na-VONTs. This confirms a bonding relaxation and a reduction in bond energy

DOI: 10.1021/acsaem.8b01895
ACS Appl. Energy Mater. 2019, 2, 822−832

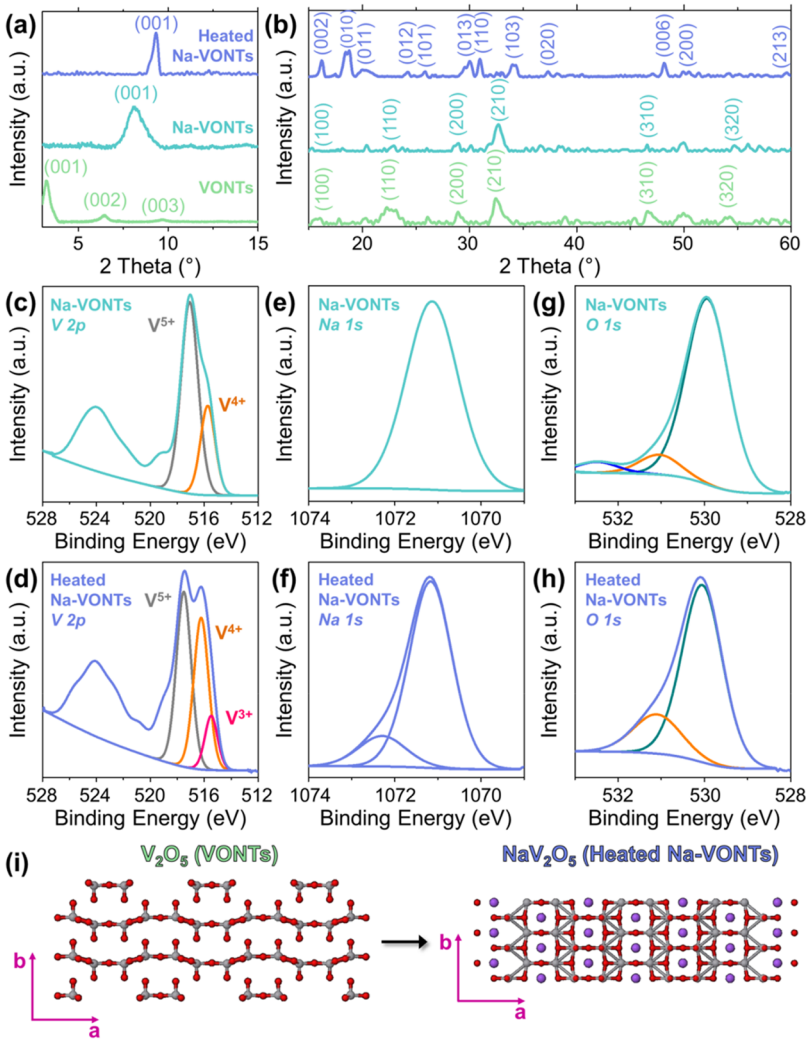

Figure 2. XRD comparison (a) (00*l*) reflections and (b) (*hk*0) reflections from as synthesized VONTs, Na-VONTs, and heated Na-VONTs. XPS spectra of the V 2p regions for (c) Na-VONTs and (d) heated Na-VONTs, Na 1s regions for (e) Na-VONTs and (f) heated Na-VONTs, and O 1s regions for (g) Na-VONTs and (h) heated Na-VONTs. (i) Unit cells for orthorhombic V_2O_5 and orthorhombic NaV_2O_5. In this representation, the orthorhombic V_2O_5 structure represents the material that constitutes each of the layers in the VONTs.

of the host lattice as a result of ion-exchange reactions and heat treatment.

The nonylamine molecules present within the vanadium oxide layers of the as-synthesized VONTs are also responsible for peaks observed in the FTIR spectra. The peaks observed at 2850 and 2920 cm^{-1} are due to symmetric and asymmetric stretching vibrations for CH_2 groups which make up the majority of the primary amine chain.[32,38−40] The other peaks observed in this region are due to symmetric and asymmetric stretching vibrations for CH_3 groups, observed at 2870 and 2955 cm^{-1}, respectively. The majority of the amine chain consists of CH_2 groups, with a single CH_3 group at its tail; hence, it would be expected that absorption peaks for the CH_2 groups would have a higher intensity in the resulting FTIR spectrum. This has been verified and can be seen in Figure 1h. The wide band observed from 3050−3250 cm^{-1} is due to N−H vibrations present from the NH_2 headgroup of the amine chain.[41] Weak peaks due to symmetric and asymmetric stretching vibrations for CH_2 and CH_3 groups are still present in the FTIR spectrum for Na-VONTs (Figure S2), indicating that there is still a low quantity of amine molecules present after the ion-exchange reaction. None of the peaks associated with the presence of amine molecules remain after their complete removal during thermal treatment. The bands observed for as-synthesized VONTs from 1550−1650 cm^{-1} and 3300−3600 cm^{-1} are assigned to O−H bending and stretching vibrations, respectively.[37,42]

XRD patterns for VONTs, Na-VONTs, and heated Na-VONTs are shown in Figure 2a,b. After hydrothermal treatment, amines are intercalated between the vanadium oxide layers and VONTs are formed; the *d*-spacing for as-synthesized VONTs from the 2Θ position of the (001) Bragg reflection corresponds to ∼2.73 nm. After ion-exchange, the majority of the nonylamine molecules have been replaced with Na^+ ions. The length of a single nonylamine molecule is ∼1.33 nm, and the ionic radius of Na^+ is ∼0.12 nm. Hence, there is a decrease in the interlayer spacing for the ion-exchanged product, and this contraction perturbs the crystal structure associated with the van der Waals layering (low angle reflections) also identified by vibrational spectroscopy earlier. The resulting interlayer spacing for scrolled Na-VONTs is ∼1.09 nm. When recrystallized to NaV_2O_5, the layering is replaced with a single crystal ladder-structured compounds as NaV_2O_5 (Figure 2b).

DOI: 10.1021/acsaem.8b01895
ACS Appl. Energy Mater. 2019, 2, 822−832

Table 1. XPS Binding Energies for Fitted Peaks (in eV)[a]

	V $2p_{3/2}$				
sample	V(V)	V(IV)	V(III)	O 1s	Na 1s
Na-VONTs	517.1 (0.70)	515.8 (0.30)		529.9	1071.2
heated Na-VONTs	517.5 (0.47)	516.3 (0.39)	515.5 (0.14)	530.1	1071.5

[a]The relative amounts of each vanadium oxidation state are shown in parentheses.

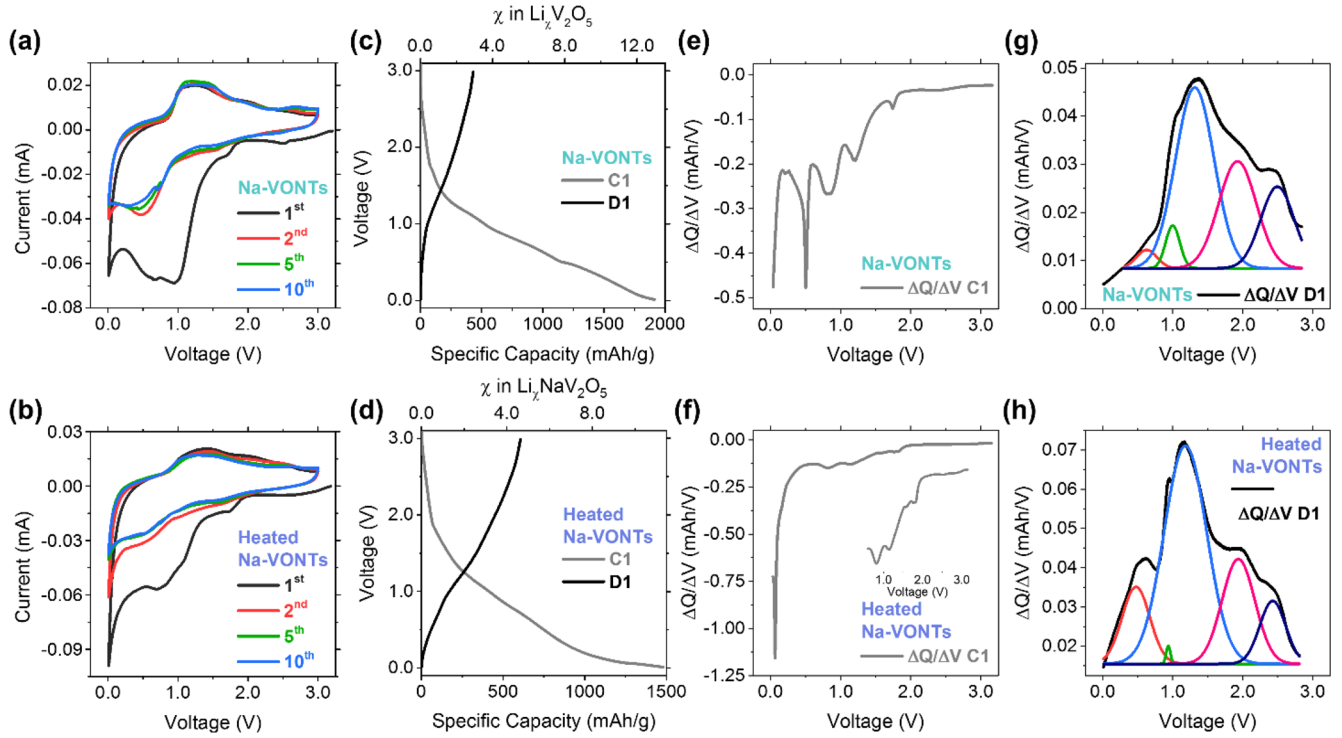

Figure 3. Cyclic voltammograms showing the 1st, 2nd, 5th, and 10th cycles, for (a) Na-VONTs and (b) heated Na-VONTs, cycled in a potential window from 3.0−0.01 V at a scan rate of 0.1 mV/s. Charge and discharge voltage profiles of the 1st cycle for (c) Na-VONTs and (d) heated Na-VONTs, cycled at a specific current of 50 mA/g in a potential window of 3.0−0.01 V (vs Li/Li^+). Differential capacity plots calculated from the 1st charge curve for (e) Na-VONTs and (f) heated Na-VONTs and from the 1st discharge curve for (g) Na-VONTs and (h) heated Na-VONTs.

The high angle XRD pattern observed for the as-prepared VONTs (Figure 2b) is in close agreement with previously reported XRD patterns for VONT samples prepared with primary amines of different chain lengths.[5,43,44] The Na^+ ions within the layers of vanadium oxide in the Na-VONTs are electrostatically bound, and their introduction does not induce any significant changes in the crystal structure of the vanadium oxide layers. Consequently, the XRD pattern for Na-VONTs is a close match to the pattern observed for the as-synthesized VONTs. A similar trend has been reported for other metal cation-exchanged VONT samples including Fe-VONTs, Co-VONTs, and Mn-VONTs.[41,45,46] However, when Na-VONTs are heated to 600 °C in N_2, the resulting XRD pattern is considerably different. This indicates that during thermal treatment a significant structural rearrangement occurs within the vanadium oxide crystal lattice. The reflections observed for the heated Na-VONTs can be indexed to pure orthorhombic NaV_2O_5 (JCPDS No. 98-000-0993) with a *Pmn*21 space group. A comparison between the XRD pattern observed for the heated Na-VONTs and the reference pattern for NaV_2O_5 is shown in Figure S3. As the Na-VONTs are heated to 600 °C, Na^+ ions may diffuse into the vanadium oxide crystal structure, resulting in the formation of a binary metal oxide. This conversion from V_2O_5 to NaV_2O_5 is in close agreement with observations from ED patterns shown in Figure 1.

X-ray photoelectron spectroscopy (XPS) spectra were acquired for each material to determine the surface chemical state of Na-VONTs and to investigate the nature of the NaV_2O_5 binary metal oxide. XPS spectra demonstrating the core level binding energies for V $2p_{3/2}$ and V $2p_{1/2}$ for Na-VONTs and heated Na-VONTs are shown in Figures 2c and 2d, respectively, and summarized in Table 1. The V 2p core levels for both samples were deconvoluted to determine the vanadium oxidation states after ion-exchange and annealing. The V $2p_{3/2}$ core level for Na-VONTs consists of two deconvoluted peaks at ~517.1 and 515.8 eV, which correspond to the presence of V^{5+} and V^{4+}, respectively.[47,48] After heating in a N_2 atmosphere, the V present within the Na-VONTs was partially reduced, and photoemission corresponding to V^{3+} was observed in the V $2p_{3/2}$ core level for heated Na-VONTs in Figure 2d. Initially ~70% of the V present in the Na-VONTs was in the V^{5+} oxidation state; this decreased to ~47% and agrees with previous reports on the reduction of vanadium oxides via annealing under inert conditions.[49,50]

The Na 1s spectra for Na-VONTs and heated Na-VONTs are shown in Figures 2e and 2f, respectively. The presence of this peak in the spectrum for Na-VONTs confirms that the

DOI: 10.1021/acsaem.8b01895
ACS Appl. Energy Mater. 2019, 2, 822−832

ion-exchange between Na^+ ions and nonylamine molecules was successful and hence supports evidence from FTIR analysis. Both spectra contain a strong peak at ~1071.2 eV which is associated with the 1s core level for Na.[51] The Na 1s spectra for the heated Na-VONTs contained a second, lower intensity peak at ~1072.3 eV and closely agrees with the reported Na 1s core level for Na_2O.[52] This indicates that there may be low levels of Na_2O present on the surface of the heated Na-VONTs. However, no reflections associated with Na_2O were observed in the XRD pattern for heated Na-VONTs, suggesting a negligible Na_2O quantity or an amorphous phase. The at. % determined from XPS does not indicate a significant quantity of Na_2O. The high-resolution spectra for the O 1s region for both Na-VONTs and heated Na-VONTs contained two oxygen contributions, as shown in Figure 2g,h. The peak at ~531.4 eV may be associated with defects and a number of surface species including hydroxyls, chemisorbed oxygen, or undercoordinated lattice oxygen.[53,54] The peak at ~530.2 eV is typical of metal−oxygen bonds.[55,56] The structural changes that occur from as-synthesized VONTs to heated Na-VONTs are illustrated in Figure 2i. Amine molecules and Li^+ are intercalated within layers of vanadium oxide along the *c*-axis; hence, the packing cells are viewed along the *c*-axis.

NaV_2O_5 from Na^+-Exchanged VONTs as a Long-Life Li-Ion Anode. The Li^+ charge storage mechanisms for Na-VONTs and heated Na-VONTs were initially investigated via analysis of cyclic voltammetry (CV) curves, as shown in Figures 3a and 3b, respectively. The initial as-prepared VONTs are V_2O_5, and after ion-exchange there are no significant phase changes, as shown from the XRD patterns in Figure 2b. Consequently, Na-VONTs exhibit electrochemical properties similar to previous reports for V_2O_5 cathode materials; however, our Na-VONT samples are examined as an anode material and are thus cycled to a lower potential limit. It is also worth noting that our Na-VONT samples were cycled on Cu substrates, which are commonly used for anode materials. Previously reported Na-VONTs that were examined as cathode materials were cycled on Al foil substrates.[16] A series of reduction peaks were observed in the initial CV scan for Na-VONTs. The reduction peaks observed at ~2.50 and 1.70 V during the initial cathodic scan are associated with the formation of the γ-$Li_\chi V_2O_5$ and ω-$Li_\chi V_2O_5$ phases, respectively.[57] The strong, wide reduction peak centered at ~0.75 V is due to the further reduction of vanadium to lower oxidation states. A similar peak was previously observed at this potential for V_2O_3 and VO_x when cycled as an anode material.[58,59] A strong peak was observed in the cathodic scan at ~1.24 V, corresponding to the promotion of V to higher oxidation states.

There are some significant differences in the initial anodic scan for the heated Na-VONTs compared to the untreated Na-VONTs, as shown in Figure 3b. Low intensity reduction peaks are observed at ~2.60 and 1.75 V, corresponding to the initial reduction of V present within NaV_2O_5. A strong reduction peak was observed at 0.70 V, followed by a sharp reduction peak from 0.50 to 0.01 V, which is characteristic of alloying type anode materials. Similar sharp reduction peaks have been observed for Ge- and Si-based anodes.[60,61] The reduction of V to lower oxidation states will be discussed in greater detail during analysis of galvanostatic cycling curves. The initial charge and discharge curves for Na-VONTs and heated Na-VONTs, cycled with an applied specific current of 50 mA/g, are shown in Figures 3c and 3d, respectively. The large initial charge capacity, which is observed for both ion-exchanged and NaV_2O_5 materials, may be attributed to the formation of an SEI layer on the surface of the nanostructured samples as well as the formation of quasi-reversible Li_2O, during the lithiation process down to the lower potential limit of 0.01 V (vs Li/Li^+). A previous study by Swider-Lyons et al. on the influence of thermal treatment on the electrochemical performance of V_2O_5 as a cathode material suggested that annealing in an O_2/H_2O atmosphere can introduce defects, within the crystal lattice, such as cation vacancies, which may serve as additional charge-storage sites and electrochemically exchange Li ions.[62] The thermal preparation of samples may have resulted in the formation of similar defect sites, and this has been reported as a contributory reason for initially higher capacities. For practical use in commercial cells, the ICE of the Na-VONT samples would need to be improved, and this is normally achieved by prelithiation. The low ICE over the first five cycles or so represents the stabilization of lithiation similar to a prelithiation step, and once achieved, the CE remains remarkably stable.[63,64]

The initial charge capacity for Na-VONTs, 1912 mAh/g, was greater than the initial value for the heated Na-VONTs, which achieved a capacity of 1481 mAh/g. Subtle differences can be observed in the voltage profiles of the charge and discharge curves for both samples. Differential capacity plots (DCPs) were determined to further investigate the charge storage mechanism for Na-VONTs and heated Na-VONTs. The DCP of the first charge for Na-VONTs contains a series of reduction peaks, as shown in Figure 3e. The wide band centered at 2.36 V and the sharp peak at 1.73 V, have previously been reported for V_2O_5 cathode materials and correspond to the formation of γ-$Li_\chi V_2O_5$ and ω-$Li_\chi V_2O_5$ phases, respectively.[57] Based on the number of moles of intercalated Li per V_2O_5 at different potentials (shown in Figure 3c), identification of $Li_\chi V_2O_5$ phases corresponding to the other reduction events are possible. The peak at 1.24 V can be attributed to the formation of a $Li_4V_2O_5$ phase and thus the reduction of V^{5+} to V^{4+}. The wide peak centered at 0.82 V corresponds to the formation of a $Li_5V_2O_5$ phase and the reduction of V^{4+} to V^{3+} and V^{2+}. At this potential (and V oxidation state), displacement reactions may possibly occur with Li_2O formation proximal to the O-deficient anode material. The sharp peak at 0.49 V may be assigned to a $Li_8V_2O_5$ phase and the reduction of V^{2+} to V^{1+}. The sharp peak from ~0.32 to 0.01 V may correspond to the reduction of V^{1+} to metallic V. Previous reports on V_2O_3 as an anode material suggest that when cycled down to 0.01 V (vs Li/Li^+), the oxide is reduced to vanadium metal and thus behaves as a conversion mode material.[65,66] The DCP for the initial recharge curve for Na-VONTs (Figure 3g) can be deconvoluted to demonstrate contributions from five oxidation peaks, which may correspond to the progressive oxidation of V from V^0 to V^{5+}, confirming efficient reoxidation of V in each cycle, deintercalation of Li, and presumably a reasonably fast oxygen mobility between the Li_2O and the suboxide, if this phase is present. The DCP of the first charge for the heated Na-VONTs (Figure 3f) contains a series of peaks at ~1.62, 1.15, 0.82, and 0.27 V, corresponding to the progressive reduction of V^{5+} to V^{1+}. The sharp peak centered at 0.05 V may be attributed to the reduction of V^{1+} to metallic V. The DCP of the initial discharge for heated Na-VONTs (Figure 3h) consisted of a series of convoluted peaks

DOI: 10.1021/acsaem.8b01895
ACS Appl. Energy Mater. 2019, 2, 822−832

at 0.47, 0.93, 1.18, 1.93, and 2.43 V, corresponding to the gradual oxidation of V to V^{5+}.

The rate response at low specific current (C-rate) of Na-VONTs and heated Na-VONTs was compared by cycling samples at an applied specific current of 50 mA/g for 250 cycles. A selection of the resulting charge and discharge profiles from the second cycle onward is shown in Figure 4. After the second charge ~3.59 mol of Li was inserted into the Na-VONTs; this decreased to ~1.75 mol after the 50th charge and decreased further to ~0.97 mol after the 250th charge. The heated Na-VONTs demonstrated a higher intercalated Li mole fraction per NaV_2O_5 unit than the Na-VONTs per V_2O_5 unit, as shown in Figure 4c,d. After the second charge ~4.63 mol of Li was inserted into the heated Na-VONTs; this value decreased to ~2.26 mol after the 50th charge and to ~1.20 mol after the 250th charge. The increase in the amount of intercalated Li leads to slightly increased capacities observed for the heated Na-VONTs compared to the ion-exchanged Na-VONTs, as shown in Figure 4e.

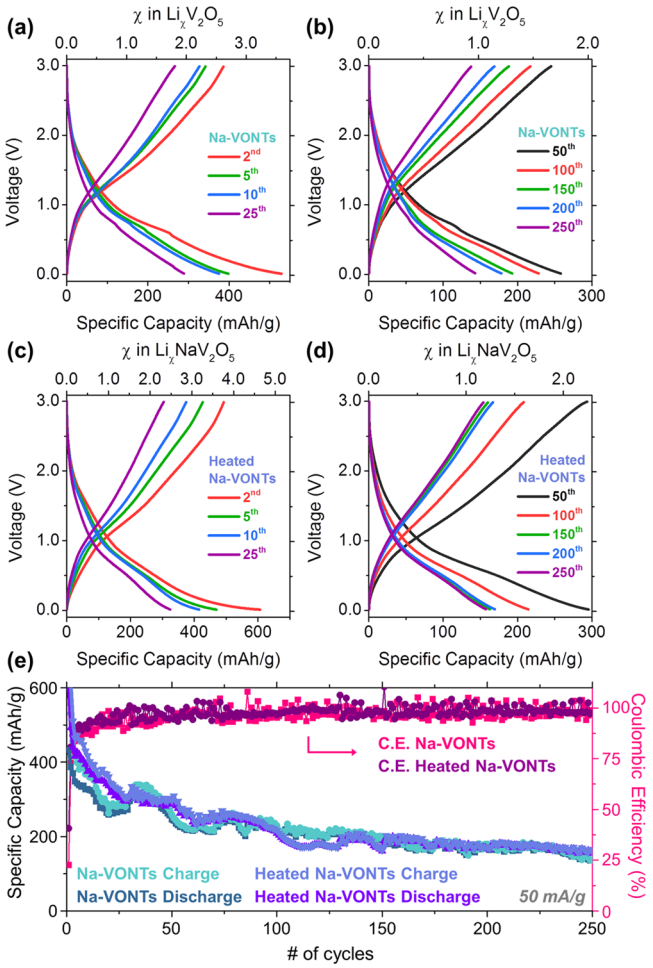

Figure 4. Charge and discharge voltage profiles for (a) the 2nd, 5th, 10th, and 25th cycles and (b) the 50th, 100th, 150th, 200th, and 250th cycles for Na-VONTs. Charge and discharge voltage profiles for (c) the 2nd, 5th, 10th, and 25th cycles and (d) the 50th, 100th, 150th, 200th, and 250th cycles for heated Na-VONTs. Na-VONTs and heated Na-VONTs were cycled at a specific current of 50 mA/g in a potential window of 3.0–0.01 V (vs Li/Li^+). (e) Comparison of the specific capacity values and Coulombic efficiency obtained for Na-VONTs and heated Na-VONTs over 250 cycles.

Both materials demonstrated similar capacity retention when cycled using a low applied specific current of 50 mA/g. Both samples demonstrated an initial sudden decrease in capacity values over the first 50 cycles; however, capacity retention significantly improved from this point onward with the Coulombic efficiencies for both samples increasing to 95–98% and remaining above this value for the remainder of the 250 cycles. Detailed analysis of the DCPs of the charge and discharge curves for both samples suggests that at lower potentials the V present in the Na-VONTs and heated Na-VONTs (NaV_2O_5) is reduced. This indicates that both samples initially behave as intercalation mode anode materials. In the case where a sufficient mole fraction of Li is intercalated to reduce the V, we surmise that at those lower potentials (<0.2 V) conversion mode processes may occur. In that case, the overall process is presumed to follow $NaV_2O_5 + zLi^+ + ze^- \rightarrow y(Na,Li)_2O + Li_xV_2O_{5-y}$, where $(Na,Li)_2O$ species form below 0.2 V following polarization effects noted in the rate of voltage drop in galvanostatic curves from 0.2 to 0.01 V. Capacity fading issues over initial cycles are well-known for conversion mode materials, and similar trends have been reported for materials including Co_3O_4, Fe_2O_3, and Mn_3O_4.[66−68] The initial irreversible capacity loss for both samples is due to the significant change in the phase of the starting materials, from a complex compound in the form of V_2O_5 or NaV_2O_5 to an unary metal. The heated Na-VONTs demonstrated slightly higher specific capacities than the Na-VONTs. After the 50th charge the specific capacity for the heated Na-VONTs was ~297 mAh/g compared to ~258 mAh/g for Na-VONTs. Similarly, the charge capacities after the 250th cycle were ~160 and 136 mAh/g for the heated Na-VONTs and Na-VONTs, respectively. Considering the stability of the cycled $Li_xNaV_2O_5$ phase toward reversible lithium intercalation and mitigation of continued capacity fading, we propose the following overall reaction suggested by Bouhedja et al.,[69] which is primarily an intercalation mode process involving lithiation of the NaV_2O_5: $Na(V^{5+}V^{4+}V^{3+}V^{2+}V^{+})O_5 + xLi^+ + xe^- \rightarrow Li_xNa(V^{(1-x)+}V^{(2-x)+}V^{(3-x)+}V^{(4-x)+}V^{(5-x)+})O_5$. This process accounts for the relative quantity of V in each oxidation state at particular voltages in the overall voltage window, in the lithium mole fraction range $0 \leq x \leq 4$. From electroneutrality conditions and multiple redox of V confirmed by CV, differential capacity, and XPS, the cation redox of V charge compensates for the Li intercalation. Once stable cycling and capacity is obtained, the Li mole fraction in $Li_xNaV_2O_5$ reduces (Figure 5d,f,h) from just over $x = 4$ to lie between $x = 0.8–1.3$. In this context, the initial capacity fading could occur because the contribution of all four redox events ($V^+–V^{2+}$, $V^{2+}–V^{3+}$, etc.) becomes limited in successive cycles, and full reoxidation happens on successive recharging steps. In this type of scenario, the relative contributions of ~1 Li or 1 e^- per V redox becomes predominantly the $V^{4+}–V^{5+}$ redox according to $Na(V^{5+}V^{4+})O_5 + xLi^+ + xe^- \rightarrow Li_xNa(V^{(4-x)+}V^{(5-x)+})O_5$.

Heated Na-VONTs demonstrated slightly higher capacity values than the Na-VONTs when cycled at a low specific current of 50 mA/g. To determine the influence of charging rate on the charge storage properties of the samples, the applied specific current was increased by a factor of 4, from 50 to 200 mA/g. Na-VONTs and heated Na-VONTs were cycled 1000 times, and a selection of charge and discharge curves from the first to the 1000th are shown in Figure 5. The voltage profiles for both samples are similar to those observed when

DOI: 10.1021/acsaem.8b01895
ACS Appl. Energy Mater. 2019, 2, 822–832

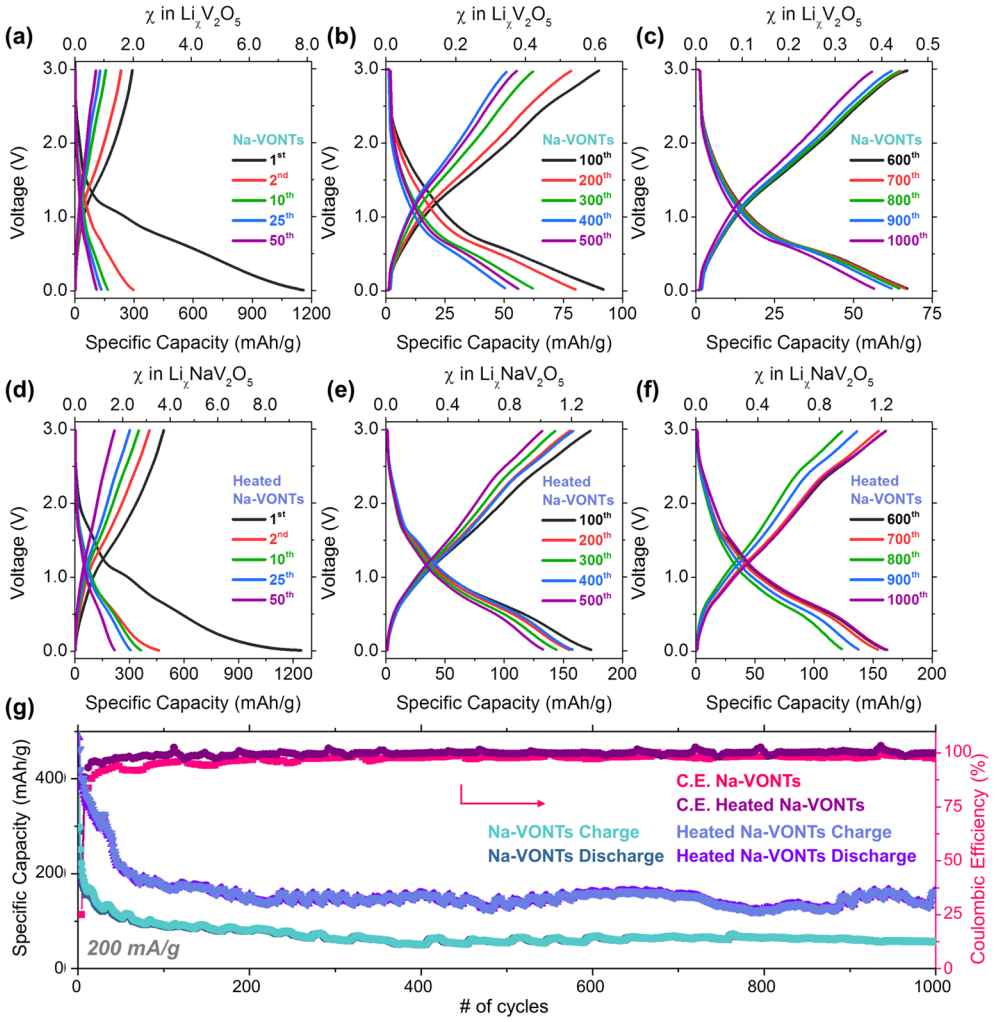

Figure 5. Charge and discharge voltage profiles for (a) the 1st, 2nd, 10th, 10th, 25th, and 50th cycles, (b) the 100th, 200th, 300th, 400th, and 500th cycles, and (c) the 600th, 700th, 800th, 900th, and 1000th cycles for Na-VONTs. Charge and discharge voltage profiles for (d) the 1st, 2nd, 10th, 10th, 25th, and 50th cycles, (e) the 100th, 200th, 300th, 400th, and 500th cycles, and (f) the 600th, 700th, 800th, 900th, and 1000th cycles for heated Na-VONTs. Na-VONTs and heated Na-VONTs were cycled at a specific current of 200 mA/g in a potential window of 3.0−0.01 V (vs Li/Li$^+$). (g) Comparison of the specific capacity values and Coulombic efficiency obtained for Na-VONTs and heated Na-VONTs over 1000 cycles.

cycled using a lower applied specific current (Figure 4). It is clear from Figure 5 that a greater mole fraction of Li was intercalated into the Na-VONTs after heating. After the 50th cycle ∼0.74 mol of Li per V_2O_5 unit was intercalated into the Na-VONTs compared to ∼1.67 mol of Li per NaV_2O_5 unit for the heated Na-VONTs. After 1000 cycles ∼0.38 and ∼1.23 mol of Li were intercalated into the Na-VONTs and heated Na-VONTs, respectively.

The greater Li insertion mole fraction for the NaV_2O_5 compared to the ion-exchanged Na-VONTs was also reflected in the specific capacity values achieved for both samples over the course of 1000 cycles. When cycled with a low applied specific current of 50 mA/g the heated Na-VONTs demonstrated slightly higher capacities than the ion-exchanged Na-VONTs; however, when cycled with a higher specific current of 200 mA/g (Figure 5g), the heated Na-VONTs exhibited considerably higher capacity values. There is an observable decrease in the capacity values over the first 100 cycles consistent with lithiation to an eventual consistent phase, before capacity retention and associated Coulombic efficiency stabilizes. This initial decrease in capacity values is common for conversion mode anode materials, but in this case the fading is eliminated in favor or efficient overall reversibility in cycling processes. The charge capacity for the heated Na-VONTs (NaV_2O_5) after 100 cycles was ∼174 mAh/g, and this decreased marginally to 162 mAh/g after the 1000th cycle; this corresponds to an impressive capacity retention of ∼93% over the course of 900 cycles for NaV_2O_5 as a negative electrode. The specific energy density of the heated Na-VONTs (NaV_2O_5) was calculated to be 261 Wh/kg (847 Wh/L based on the density of NaV_2O_5) after the 100th charge and 244 Wh/kg after the 1000th charge, which is significantly higher that the values obtained for the untreated Na-VONTs; 138 and 86 Wh/kg after the 100th and 1000th charge, respectively.

Heated Na-VONTs as NaV_2O_5 demonstrated specific capacity values that are greater than previously reported values for other vanadium oxide-based anode materials including V_2O_3, $Li_{1.1}V_{0.9}O_2$, and Li_3VO_4[14,70−76] and comparable to vanadium oxide/carbon composite anode materials such as carbon-encapsulated Li_3VO_4, Li_3VO_4/C submicrometer ellipsoids supported on reduced graphene oxide and a Li_3VO_4

DOI: 10.1021/acsaem.8b01895
ACS Appl. Energy Mater. 2019, 2, 822−832

nanoribbon/graphene composite.[77−79] A comparison of the capacity values observed for the heated Na-VONTs with charge capacities obtained for various vanadium oxide anode materials from the literature is illustrated in Figure S4 and listed in Table S1. Pseudocapacitive contributions to NaV_2O_5 formed by S^{2-}-assisted modification of crystal structure have just been reported, indicating that the nature of the morphology and synthetic route still plays a role in the basic reaction mechanism of orthorhombic and monoclinic NaV_2O_5 with Li.[80] This comparison with literature values benchmarks the results presented in this work compared to other vanadium oxide-based lower voltage anode materials and for oxides that enable intercalation of solid solutions in addition to a nanocomposite formation at very low potentials to give a stable oxide anode.

CONCLUSIONS

To prepare an oxide anode that undergoes intercalation reactions and stable cycling over 1000 cycles at a high rate, we developed a Na ion-exchange protocol for VONTs to replace the amine functionalization, in a manner that allows ∼1 Na per V_2O_5 unit to form the NaV_2O_5 phase on heating. The thermal treatment of Na-VONTs recrystallizes this nanotubular structure into irregularly shaped NaV_2O_5 crystals. The superior capacities obtained with the heated Na-VONTs compared to the untreated Na-VONTs are due to significant differences in the phase and crystal structure of the materials. We propose that the heated Na-VONTs behave as an intercalation mode material that avoids a dominant contribution to conversion modes processes from a metal oxide. Anion redox in this material is not believed to contribute to charge capacity, and lithiation is predominantly linked to the valence of the vanadium atom in the NaV_2O_5 crystal structure according to voltammetic profiling, but unequivocal determination of the anionic O redox activity in a sodium vanadate bronze intercalated by lithium remains to be determined.

Galvanostatic testing demonstrated the exceptional capacity retention properties of the heated Na-VONTs, delivering reversible capacities of ∼174 and 162 mAh/g after the 100th and 1000th cycles, respectively, at a specific current of 200 mA/g. This corresponds to an impressive capacity retention of ∼93% between the 100th and 1000th cycles. The capacity values exhibited by the NaV_2O_5 exceed most vanadium oxide-based materials tested at low potentials as anodes, including V_2O_3, $Li_{1.1}V_{0.9}O_2$, and Li_3VO_4. This shows that significantly high specific capacities can be obtained for NaV_2O_5 nanostructures over a large number of cycles with exceptional capacity retention once the stabilized cation redox and cycled lithiated phase is formed. As a conductive additive and binder-free formulation, sufficient electrical conductivity is maintained in this anode material and can be assessed at low voltage without graphite content or binder. The electrochemical performance of the heated Na-VONTs indicates that they have potential as an anode material for long cycle life Li-ion batteries, and the detailed analysis offers more insight into the development of higher volumetric energy density oxides as anode materials that are electrochemically more stable when conversion-mode processes are present.

ASSOCIATED CONTENT

Supporting Information

The Supporting Information is available free of charge on the ACS Publications website at DOI: 10.1021/acsaem.8b01895.

TEM data of bundles and individual scrolled V_2O_5 nanotubes (VONTs); FTIR spectra of the organic structure-directing amine template and the vanadate inorganic constituents; XRD pattern for the NaV_2O_5 phase; and a tabulated/graphical comparison of specific capacity values from other closely related vanadates in the literature (PDF)

AUTHOR INFORMATION

Corresponding Author

*Fax +353 21 427 4097; Tel +353 21 490 2732; e-mail c.odwyer@ucc.ie.

ORCID

David McNulty: 0000-0002-6337-3395

Colm O'Dwyer: 0000-0001-7429-015X

Notes

The authors declare no competing financial interest.

ACKNOWLEDGMENTS

This publication has emanated from research conducted with the financial support of the Charles Parsons Initiative and Science Foundation Ireland (SFI) under Grant 06/CP/E007. Part of this work was conducted under the framework of the INSPIRE programme, funded by the Irish Government's Programme for Research in Third Level Institutions, Cycle 4, National Development Plan 2007-2013. C.O.D. acknowledges support from Science Foundation Ireland under Award 14/IA/2581 and through Technology Innovation & Development Awards under Contracts 13/TIDA/E2761 and 15/TIDA/2893.

REFERENCES

(1) Spahr, M. E.; Bitterli, P.; Nesper, R.; Müller, M.; Krumeich, F.; Nissen, H. U. Redox Active Nanotubes of Vanadium Oxide. *Angew. Chem., Int. Ed.* **1998**, *37*, 1263−1265.

(2) Nordlinder, S.; Edström, K.; Gustafsson, T. The Performance of Vanadium Oxide Nanorolls as Cathode Material in a Rechargeable Lithium Battery. *Electrochem. Solid-State Lett.* **2001**, *4*, A129−A131.

(3) Nordlinder, S.; Nyholm, L.; Gustafsson, T.; Edström, K. Lithium Insertion into Vanadium Oxide Nanotubes: Electrochemical and Structural Aspects. *Chem. Mater.* **2006**, *18*, 495−503.

(4) Kim, J.-K.; Senthilkumar; Sahgong, S. H.; Kim, J.-H.; Chi, M.; Kim, Y. New chemical route for the synthesis of beta-$Na_{0.33}V_2O_5$ and its fully reversible Li intercalation. *ACS Appl. Mater. Interfaces* **2015**, *7*, 7025−7032.

(5) Liu, P.; Zhu, K.; Gao, Y.; Luo, H.; Lu, L. Recent Progress in the Applications of Vanadium-Based Oxides on Energy Storage: from Low-Dimensional Nanomaterials Synthesis to 3D Micro/Nano-Structures and Free-Standing Electrodes Fabrication. *Adv. Energy Mater.* **2017**, *7*, 1700547.

(6) Liu, P.; Zhou, D.; Zhu, K.; Wu, Q.; Wang, Y.; Tai, G.; Zhang, W.; Gu, Q. Bundle-like alpha'-NaV_2O_5 mesocrystals: from synthesis, growth mechanism to analysis of Na-ion intercalation/deintercalation abilities. *Nanoscale* **2016**, *8*, 1975−1985.

(7) Spahr, M. E.; Stoschitzki Bitterli, P.; Nesper, R.; Haas, O.; Novák, P. Vanadium Oxide Nanotubes. A New Nanostructured Redox-Active Material for the Electrochemical Insertion of Lithium. *J. Electrochem. Soc.* **1999**, *146*, 2780−2783.

(8) Muhr, H. J.; Krumeich, F.; Schönholzer, U. P.; Bieri, F.; Niederberger, M.; Gauckler, L. J.; Nesper, R. Vanadium Oxide Nanotubes - a New Flexible Vanadate Nanophase. *Adv. Mater.* **2000**, *12*, 231−234.

(9) Krumeich, F.; Muhr, H. J.; Niederberger, M.; Bieri, F.; Schnyder, B.; Nesper, R. Morphology and Topochemical Reactions of Novel

Vanadium Oxide Nanotubes. *J. Am. Chem. Soc.* **1999**, *121*, 8324−8331.
(10) Niederberger, M.; Muhr, H.-J.; Krumeich, F.; Bieri, F.; Günther, D.; Nesper, R. Low-Cost Synthesis of Vanadium Oxide Nanotubes Via Two Novel Non-Alkoxide Routes. *Chem. Mater.* **2000**, *12*, 1995−2000.
(11) Popa, A. I.; Vavilova, E.; Täschner, C.; Kataev, V.; Büchner, B.; Klingeler, R. D. Electrochemical Behavior and Magnetic Properties of Vanadium Oxide Nanotubes. *J. Phys. Chem. C* **2011**, *115*, 5265−5270.
(12) McNulty, D.; Buckley, D. N.; O'Dwyer, C. Structural and Electrochemical Characterization of Thermally Treated Vanadium Oxide Nanotubes for Li-Ion Batteries. *ECS Trans.* **2013**, *50*, 165−174.
(13) McNulty, D.; Buckley, D. N.; O'Dwyer, C. V_2O_3 Polycrystalline Nanorod Cathode Materials for Li-Ion Batteries with Long Cycle Life and High Capacity Retention. *ChemElectroChem.* **2017**, *4*, 2037−2044.
(14) Armstrong, A. R.; Lyness, C.; Panchmatia, P. M.; Islam, M. S.; Bruce, P. G. The Lithium Intercalation Process in the Low-Voltage Lithium Battery Anode $Li_{1+X}V_{1-X}O_2$. *Nat. Mater.* **2011**, *10*, 223−229.
(15) McNulty, D.; Collins, G.; O'Dwyer, C. $NiVO_3$ Fused Oxide Nanoparticles − an Electrochemically Stable Intercalation Anode Material for Lithium Ion Batteries. *J. Mater. Chem. A* **2018**, *6*, 18103.
(16) Nordlinder, S.; Lindgren, J.; Gustafsson, T.; Edström, K. The Structure and Electrochemical Performance of Na^+, K^+, and Ca^{2+}-Vanadium Oxide Nanotubes. *J. Electrochem. Soc.* **2003**, *150*, E280−E284.
(17) Zhou, X.; Wu, G.; Gao, G.; Wang, J.; Yang, H.; Wu, J.; Shen, J.; Zhou, B.; Zhang, Z. Electrochemical Performance Improvement of Vanadium Oxide Nanotubes as Cathode Materials for Lithium Ion Batteries through Ferric Ion Exchange Technique. *J. Phys. Chem. C* **2012**, *116*, 21685−21692.
(18) Maggay, I. V. B.; De Juan, L. M. Z.; Lu, J.-S.; Nguyen, M. T.; Yonezawa, T.; Chan, T.-S.; Liu, W.-R. Electrochemical Properties of Novel Fev2o4 as an Anode for Na-Ion Batteries. *Sci. Rep.* **2018**, *8*, 8839.
(19) Zhang, L.; Zhao, K.; Luo, Y.; Dong, Y.; Xu, W.; Yan, M.; Ren, W.; Zhou, L.; Qu, L.; Mai, L. Acetylene Black Induced Heterogeneous Growth of Macroporous CoV_2O_6 Nanosheet for High-Rate Pseudocapacitive Lithium-Ion Battery Anode. *ACS Appl. Mater. Interfaces* **2016**, *8*, 7139−7146.
(20) Chen, X.; Sun, X.; Li, Y. Self-Assembling Vanadium Oxide Nanotubes by Organic Molecular Templates. *Inorg. Chem.* **2002**, *41*, 4524−4530.
(21) Chandrappa, G. T.; Steunou, N.; Cassaignon, S.; Bauvais, C.; Livage, J. Hydrothermal Synthesis of Vanadium Oxide Nanotubes from V_2O_5 Gels. *Catal. Today* **2003**, *78*, 85−89.
(22) McNulty, D.; Buckley, D. N.; O'Dwyer, C. Synthesis and Characterization of Layered Vanadium Oxide Nanotubes for Rechargeable Lithium Batteries. *ECS Trans.* **2011**, *35*, 237−245.
(23) McNulty, D.; Buckley, D. N.; O'Dwyer, C. Optimizing the Structure and Yield of Vanadium Oxide Nanotubes by Periodic 2D Layer Scrolling. *RSC Adv.* **2016**, *6*, 40932−40944.
(24) McNulty, D.; Buckley, D. N.; O'Dwyer, C. Vanadium Oxide Polycrystalline Nanorods and Ion-Exchanged Nanotubes for Enhanced Lithium Intercalation. *ECS Trans.* **2015**, *64*, 1−12.
(25) McNulty, D.; Buckley, D. N.; O'Dwyer, C. Synthesis and Electrochemical Properties of Vanadium Oxide Materials and Structures as Li-Ion Battery Positive Electrodes. *J. Power Sources* **2014**, *267*, 831−873.
(26) O'Dwyer, C.; Lavayen, V.; Tanner, D. A.; Newcomb, S. B.; Benavente, E.; Gonzalez, G.; Sotomahyor Torres, C. M. Reduced Surfactant Uptake in Three Dimensional Assemblies of VO(x) Nanotubes Improves Reversible Li^+ Intercalation and Charge Capacity. *Adv. Funct. Mater.* **2009**, *19*, 1736−1745.
(27) Liu, P.; Moudrakovski, I. L.; Liu, J.; Sayari, A. Mesostructured Vanadium Oxide Containing Dodecylamine⊥. *Chem. Mater.* **1997**, *9*, 2513−2520.
(28) Reinoso, J. M.; Muhr, H. J.; Krumeich, F.; Bieri, F.; Nesper, R. Controlled Uptake and Release of Metal Cations by Vanadium Oxide Nanotubes. *Helv. Chim. Acta* **2000**, *83*, 1724−1733.
(29) Cao, J.; Musfeldt, J.; Mazumdar, S.; Chernova, N.; Whittingham, M. Pinned Low-Energy Electronic Excitation in Metal-Exchanged Vanadium Oxide Nanoscrolls. *Nano Lett.* **2007**, *7*, 2351−2355.
(30) Malta, M.; Louarn, G.; Errien, N.; Torresi, R. M. Redox Behavior of Nanohybrid Material with Defined Morphology: Vanadium Oxide Nanotubes Intercalated with Polyaniline. *J. Power Sources* **2006**, *156*, 533−540.
(31) McNulty, D.; Buckley, D.; O'Dwyer, C. Polycrystalline Vanadium Oxide Nanorods: Growth, Structure and Improved Electrochemical Response as a Li-Ion Battery Cathode Material. *J. Electrochem. Soc.* **2014**, *161*, A1321−A1329.
(32) Chen, W.; Peng, J.; Mai, L.; Zhu, Q.; Xu, Q. Synthesis of Vanadium Oxide Nanotubes from V_2o_5 Sols. *Mater. Lett.* **2004**, *58*, 2275−2278.
(33) Azambre, B.; Hudson, M.; Heintz, O. Topotactic Redox Reactions of Copper (Ii) and Iron (Iii) Salts within Vox Nanotubes. *J. Mater. Chem.* **2003**, *13*, 385−393.
(34) Liu, H.; Wang, Y.; Li, L.; Wang, K.; Hosono, E.; Zhou, H. Facile Synthesis of Nav6o15 Nanorods and Its Electrochemical Behavior as Cathode Material in Rechargeable Lithium Batteries. *J. Mater. Chem.* **2009**, *19*, 7885−7891.
(35) Liu, H.; Zhou, H.; Chen, L.; Tang, Z.; Yang, W. Electrochemical Insertion/Deinsertion of Sodium on NaV_6O_{15} Nanorods as Cathode Material of Rechargeable Sodium-Based Batteries. *J. Power Sources* **2011**, *196*, 814−819.
(36) Zhou, G.-T.; Wang, X.; Yu, J. C. Selected-Control Synthesis of NaV_6O_{15} and $Na_2V_6O_{16}$. $3H_2O$ Single-Crystalline Nanowires. *Cryst. Growth Des.* **2005**, *5*, 969−974.
(37) Sabbar, E.; De Roy, M.; Besse, J. Synthetic Pathways to New Hydrated Sodium and Lithium Vanadium Bronzes. *J. Solid State Chem.* **2000**, *149*, 443−448.
(38) Liu, J.; Wang, X.; Peng, Q.; Li, Y. Vanadium Pentoxide Nanobelts: Highly Selective and Stable Ethanol Sensor Materials. *Adv. Mater.* **2005**, *17*, 764−767.
(39) O'Dwyer, C.; Gannon, G.; McNulty, D.; Buckley, D. N.; Thompson, D. Accommodating Curvature in a Highly Ordered Functionalized Metal Oxide Nanofiber: Synthesis, Characterization, and Multiscale Modeling of Layered Nanosheets. *Chem. Mater.* **2012**, *24*, 3981−3992.
(40) Sediri, F.; Touati, F.; Gharbi, N. A One-Step Hydrothermal Way for the Synthesis of Vanadium Oxide Nanotubes Containing the Phenylpropylamine as Template Obtained Via Non-Alkoxide Route. *Mater. Lett.* **2007**, *61*, 1946−1950.
(41) Dobley, A.; Ngala, K.; Yang, S.; Zavalij, P. Y.; Whittingham, M. S. Manganese Vanadium Oxide Nanotubes: Synthesis, Characterization, and Electrochemistry. *Chem. Mater.* **2001**, *13*, 4382−4386.
(42) Vera-Robles, L.; Naab, F.; Campero, A.; Duggan, J.; McDaniel, F. Metal Cations Inserted in Vanadium-Oxide Nanotubes. *Nucl. Instrum. Methods Phys. Res., Sect. B* **2007**, *261*, 534−537.
(43) Cui, C.-J.; Wu, G.-M.; Yang, H.-Y.; She, S.-F.; Shen, J.; Zhou, B.; Zhang, Z.-H. A New High-Performance Cathode Material for Rechargeable Lithium-Ion Batteries: Polypyrrole/Vanadium Oxide Nanotubes. *Electrochim. Acta* **2010**, *55*, 8870−8875.
(44) Sharma, S.; Thomas, J.; Ramanan, A.; Panthöfer, M.; Jansen, M. Hydrothermal Synthesis of Vanadium Oxide Nanotubes from Oxide Precursors. *J. Nanosci. Nanotechnol.* **2007**, *7*, 1985−1989.
(45) Zakharova, G. S.; Liu, Y.; Enyashin, A. N.; Yang, X.; Zhou, J.; Jin, W.; Chen, W. Metal Cations Doped Vanadium Oxide Nanotubes: Synthesis, Electronic Structure, and Gas Sensing Properties. *Sens. Actuators, B* **2018**, *256*, 1021−1029.
(46) Zhang, K.; Gao, G.; Sun, W.; Liang, X.; Liu, Y.; Wu, G. Large Interlayer Spacing Vanadium Oxide Nanotubes as Cathodes for High Performance Sodium Ion Batteries. *RSC Adv.* **2018**, *8*, 22053−22061.
(47) Silversmit, G.; Depla, D.; Poelman, H.; Marin, G. B.; De Gryse, R. Determination of the V2p Xps Binding Energies for Different

DOI: 10.1021/acsaem.8b01895
ACS Appl. Energy Mater. 2019, 2, 822−832

Vanadium Oxidation States (V^{5+} to V^{0+}). *J. Electron Spectrosc. Relat. Phenom.* **2004**, *135*, 167−175.
(48) Wei, Q.; Liu, J.; Feng, W.; Sheng, J.; Tian, X.; He, L.; An, Q.; Mai, L. Hydrated Vanadium Pentoxide with Superior Sodium Storage Capacity. *J. Mater. Chem. A* **2015**, *3*, 8070−8075.
(49) Piao, J.; Takahashi, S.; Kohiki, S. Preparation and Characterization of V_2O_3 Powder and Film. *Jpn. J. Appl. Phys.* **1998**, *37*, 6519−6523.
(50) Ramana, C. V.; Utsunomiya, S.; Ewing, R. C.; Becker, U. Formation of V_2O_3 Nanocrystals by Thermal Reduction of V_2O_5 Thin Films. *Solid State Commun.* **2006**, *137*, 645−649.
(51) Kowalczyk, S. P.; Ley, L.; McFeely, F. R.; Pollak, R. A.; Shirley, D. A. X-Ray Photoemission from Sodium and Lithium. *Phys. Rev. B* **1973**, *8*, 3583−3585.
(52) Barrie, A.; Street, F. J. An Auger and X-Ray Photoelectron Spectroscopic Study of Sodium Metal and Sodium Oxide. *J. Electron Spectrosc. Relat. Phenom.* **1975**, *7*, 1−31.
(53) Roginskaya, Y. E.; Morozova, O. V.; Lubnin, E. N.; Ulitina, Y. E.; Lopukhova, G. V.; Trasatti, S. Characterization of Bulk and Surface Composition of $Co_xNi_{1-X}O_y$ Mixed Oxides for Electrocatalysis. *Langmuir* **1997**, *13*, 4621−4627.
(54) Zhong, J.-H.; Wang, A.-L.; Li, G.-R.; Wang, J.-W.; Ou, Y.-N.; Tong, Y.-X. $Co_3O_4/Ni(OH)_2$ Composite Mesoporous Nanosheet Networks as a Promising Electrode for Supercapacitor Applications. *J. Mater. Chem.* **2012**, *22*, 5656−5665.
(55) Marco, J. F.; Gancedo, J. R.; Gracia, M.; Gautier, J. L.; Ríos, E.; Berry, F. J. Characterization of the Nickel Cobaltite, $NiCo_2O_4$, Prepared by Several Methods: An Xrd, Xanes, Exafs, and Xps Study. *J. Solid State Chem.* **2000**, *153*, 74−81.
(56) Choudhury, T.; Saied, S. O.; Sullivan, J. L.; Abbot, A. M. Reduction of Oxides of Iron, Cobalt, Titanium and Niobium by Low-Energy Ion Bombardment. *J. Phys. D: Appl. Phys.* **1989**, *22*, 1185.
(57) Delmas, C.; Cognac-Auradou, H.; Cocciantelli, J. M.; Ménétrier, M.; Doumerc, J. P. The $Li_xv_2o_5$ System: An Overview of the Structure Modifications Induced by the Lithium Intercalation. *Solid State Ionics* **1994**, *69*, 257−264.
(58) Jia, B.-R.; Qin, M.-L.; Zhang, Z.-L.; Li, S.-M.; Zhang, D.-Y.; Wu, H.-Y.; Zhang, L.; Lu, X.; Qu, X.-H. Hollow Porous VO_x/C Nanoscrolls as High-Performance Anodes for Lithium-Ion Batteries. *ACS Appl. Mater. Interfaces* **2016**, *8*, 25954−25961.
(59) Xiao, B.; Zhang, B.; Tang, L.-B.; An, C.-S.; He, Z.-J.; Tong, H.; Yu, W.-J.; Zheng, J.-C. V_2O_3/rGO Composite as a Potential Anode Material for Lithium Ion Batteries. *Ceram. Int.* **2018**.
(60) Stokes, K.; Geaney, H.; Flynn, G.; Sheehan, M.; Kennedy, T.; Ryan, K. M. Direct Synthesis of Alloyed Si1−Xgex Nanowires for Performance-Tunable Lithium Ion Battery Anodes. *ACS Nano* **2017**, *11*, 10088−10096.
(61) McNulty, D.; Geaney, H.; Buckley, D.; O'Dwyer, C. High Capacity Binder-Free Nanocrystalline GeO2 Inverse Opal Anodes for Li-Ion Batteries with Long Cycle Life and Stable Cell Voltage. *Nano Energy* **2018**, *43*, 11−21.
(62) Swider-Lyons, K. E.; Love, C. T.; Rolison, D. R. Improved Lithium Capacity of Defective V2o5Materials. *Solid State Ionics* **2002**, *152−153*, 99−104.
(63) Liu, N.; Hu, L.; McDowell, M. T.; Jackson, A.; Cui, Y. Prelithiated Silicon Nanowires as an Anode for Lithium Ion Batteries. *ACS Nano* **2011**, *5*, 6487−6493.
(64) Forney, M. W.; Ganter, M. J.; Staub, J. W.; Ridgley, R. D.; Landi, B. J. Prelithiation of Silicon−Carbon Nanotube Anodes for Lithium Ion Batteries by Stabilized Lithium Metal Powder (Slmp). *Nano Lett.* **2013**, *13*, 4158−4163.
(65) Dong, Y.; Ma, R.; Hu, M.; Cheng, H.; Lee, J.-M.; Li, Y. Y.; Zapien, J. A. Polymer-Pyrolysis Assisted Synthesis of Vanadium Trioxide and Carbon Nanocomposites as High Performance Anode Materials for Lithium-Ion Batteries. *J. Power Sources* **2014**, *261*, 184−187.
(66) Jiang, H.; Jia, G.; Hu, Y.; Cheng, Q.; Fu, Y.; Li, C. Ultrafine V_2O_3 Nanowire Embedded in Carbon Hybrids with Enhanced Lithium Storage Capability. *Ind. Eng. Chem. Res.* **2015**, *54*, 2960−2965.
(67) McNulty, D.; Geaney, H.; Carroll, E.; Garvey, S.; Lonergan, A.; O'Dwyer, C. The Effect of Particle Size, Morphology and C-Rates on 3D Structured Co_3O_4 Inverse Opal Conversion Mode Anode Materials. *Mater. Res. Express* **2017**, *4*, No. 025011.
(68) Cao, K.; Jin, T.; Yang, L.; Jiao, L. Recent Progress in Conversion Reaction Metal Oxide Anodes for Li-Ion Batteries. *Mater. Chem. Front.* **2017**, *1*, 2213−2242.
(69) Bouhedja, L.; Castro-Garcia, S.; Livage, J.; Julien, C. M. Lithium intercalation in α'-$Na_yV_2O_5$ synthesized via the hydrothermal route. *Ionics* **1998**, *4*, 227−233.
(70) Li, X.; Fu, J.; Pan, Z.; Su, J.; Xu, J.; Gao, B.; Peng, X.; Wang, L.; Zhang, X.; Chu, P. K. Peapod-Like V_2o_3 Nanorods Encapsulated into Carbon as Binder-Free and Flexible Electrodes in Lithium-Ion Batteries. *J. Power Sources* **2016**, *331*, 58−66.
(71) Choi, N.-S.; Kim, J.-S.; Yin, R.-Z.; Kim, S.-S. Electrochemical Properties of Lithium Vanadium Oxide as an Anode Material for Lithium-Ion Battery. *Mater. Chem. Phys.* **2009**, *116*, 603−606.
(72) Li, H.; Liu, X.; Zhai, T.; Li, D.; Zhou, H. Li_3VO_4: A Promising Insertion Anode Material for Lithium-Ion Batteries. *Adv. Energy Mater.* **2013**, *3*, 428−432.
(73) Kim, W.-T.; Jeong, Y. U.; Lee, Y. J.; Kim, Y. J.; Song, J. H. Synthesis and Lithium Intercalation Properties of Li_3VO_4 as a New Anode Material for Secondary Lithium Batteries. *J. Power Sources* **2013**, *244*, 557−560.
(74) Shao, G.; Gan, L.; Ma, Y.; Li, H.; Zhai, T. Enhancing the Performance of Li_3VO_4 by Combining Nanotechnology and Surface Carbon Coating for Lithium Ion Batteries. *J. Mater. Chem. A* **2015**, *3*, 11253−11260.
(75) Zhao, D.; Cao, M. Constructing Highly Graphitized Carbon-Wrapped Li_3VO_4 Nanoparticles with Hierarchically Porous Structure as a Long Life and High Capacity Anode for Lithium-Ion Batteries. *ACS Appl. Mater. Interfaces* **2015**, *7*, 25084−25093.
(76) Ahn, J.; Oh, S. H.; Kim, J. H.; Cho, B. W.; Kim, H. S. The Effect of Vanadium Precursors on the Electrochemical Performance of $Li_{1.1}V_{0.9}O_2$ as an Anode Material for Li-Ion Batteries. *J. Electroceram.* **2014**, *32*, 390−395.
(77) Zhang, C.; Song, H.; Liu, C.; Liu, Y.; Zhang, C.; Nan, X.; Cao, G. Fast and Reversible Li Ion Insertion in Carbon-Encapsulated Li_3VO_4 as Anode for Lithium-Ion Battery. *Adv. Funct. Mater.* **2015**, *25*, 3497−3504.
(78) Li, Q.; Wei, Q.; Sheng, J.; Yan, M.; Zhou, L.; Luo, W.; Sun, R.; Mai, L. Mesoporous Li_3VO_4/C Submicron-Ellipsoids Supported on Reduced Graphene Oxide as Practical Anode for High-Power Lithium-Ion Batteries. *Adv. Sci.* **2015**, *2*, 1500284.
(79) Liu, J.; Lu, P.-J.; Liang, S.; Liu, J.; Wang, W.; Lei, M.; Tang, S.; Yang, Q. Ultrathin Li_3VO_4 Nanoribbon/Graphene Sandwich-Like Nanostructures with Ultrahigh Lithium Ion Storage Properties. *Nano Energy* **2015**, *12*, 709−724.
(80) Li, W.; Huang, J.; Cao, L.; Liu, Y.; Pan, L.; Feng, L. In Situ Topology Synthesis of Orthorhombic NaV_2O_5 with High Pseudocapacitive Contribution for Lithium-Ion Battery Anode. *ACS Sustainable Chem. Eng.* **2019**, *7*, 94.

DOI: 10.1021/acsaem.8b01895
ACS Appl. Energy Mater. 2019, 2, 822−832